

Resonant photoionization of Ni I into autoionizing states

P. Lievens, E. Vandeweert, P. Thoen, and R. E. Silverans

Laboratorium voor Vaste-Stoffysika en Magnetisme, Katholieke Universiteit Leuven, Celestijnenlaan 200D, B-3001 Leuven, Belgium

(Received 22 March 1996)

Two-step resonant photoionization of free Ni atoms is studied by one-color and two-color processes, using pulsed lasers with photon energies around half the ground-state ionization energy. Two-color two-step resonance ionization from the ground state a^3F_4 and the first metastable state a^3D_3 via the triplet states $z^3G_{3,4,5}^0$ was used to probe the autoionizing states just above the ionization limit. Several strong lines in the one-color ionization spectrum are explained as direct two-photon transitions to autoionizing states. Photoionization cross sections were deduced from saturation measurements. The large cross sections observed for specific one-color two-step transitions are due to the near double resonant excitation into autoionizing states.

[S1050-2947(96)01109-2]

PACS number(s): 32.80.Rm, 33.80.Rv, 32.80.Dz, 32.80.Fb

I. INTRODUCTION

Multistep resonant ionization spectroscopy (RIS) using pulsed lasers has proven its usefulness and versatility in various physical and chemical applications [1]. Benefit is taken of the large sensitivity and the inherent element selectivity of RIS; for example, in trace analysis, surface analysis studies, and highly efficient laser ion sources. In many cases, especially for the study of elements with high ionization potentials, several photons with different energies are needed to ionize the atoms. This requires the availability of rather complicated laser setups and can seriously hamper the routine application of RIS. One of the most frequently employed resonance ionization schemes is the so-called two-color two-step process with the first step (excitation) tuned to a strong atomic transition, and the second step (ionization) resonant to an autoionizing state [2,3]. This implies the use of two tunable and synchronized laser systems. In some cases this scheme can be simplified by using the same photon energy for both the excitation and the ionization step (one-color two-step process). However, this often leads to a much lower ionization cross section and therefore also to a significant reduction in ionization efficiency. Only if the frequency of the resonant excitation step precisely matches a transition from the excited state into an autoionizing state, will the ionization cross section be optimum. Furthermore, since the cross section for ionization is largest just above the first ionization limit, the excitation step and thus also the intermediate level should be chosen at an energy just above half the ionization potential.

Our study of resonance ionization of Ni is related to two different RIS applications. The first one is the production of ion beams of short-lived isotopes far from stability by means of a laser ion source. For the efficient production of contaminant-free Ni ion beams, maximum benefit was taken from the experimental simplicity of the one-color two-step resonant ionization scheme for Ni [4,5]. A second research topic is the study of the atomization processes of metals (e.g., Ni and Co) during energetic beam-solid interactions (i.e., ion beam sputtering or laser ablation). In such atomization processes, several excited states of the neutral atom are populated, apart from the production of ions and neutral or

charged clusters. Resonance ionization spectroscopy offers a sensitive experimental tool for determining the population of the metastable states [6,7].

In this paper we will compare the photoionization of Ni by one-color and two-color two-step processes using laser photon energies around half the ground-state ionization energy. The experimental apparatus is briefly described in Sec. II. In Sec. III, we first treat one-color resonant ionization. Next, the determination of autoionizing states near the first ionization limit is presented and used to interpret the one-color two-step ionization spectrum. Finally, saturation measurements are reported from which ionization cross sections are deduced. These are discussed in view of the enhancement of photoionization efficiencies for processes involving autoionizing states.

II. EXPERIMENTAL SETUP

The experiments were performed with a resonance ionization mass spectrometry setup, schematically presented in Fig. 1. Ni atoms are produced in ultrahigh vacuum ($\sim 10^{-9}$ hPa) by continuous sputtering of a polycrystalline Ni foil (purity 99.9%) with 12-keV Ar ions (ion beam current about 1.6 μ A) at 45° incidence angle. The plume of atomized atoms is then irradiated by tunable UV laser light about 3 mm above the sample. The Ni atoms are ionized by one- or two-color two-step processes and electrostatically extracted and focused into a reflectron time-of-flight spectrometer, where they are detected mass selectively with a mass resolution of

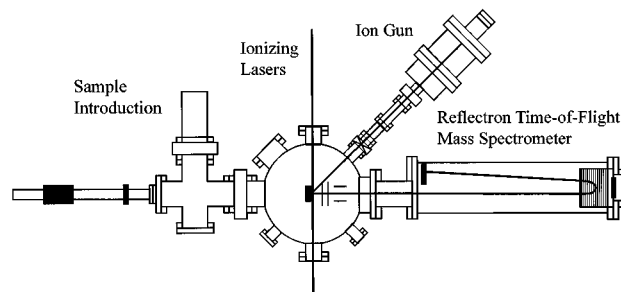


FIG. 1. Resonance ionization mass spectrometry setup.

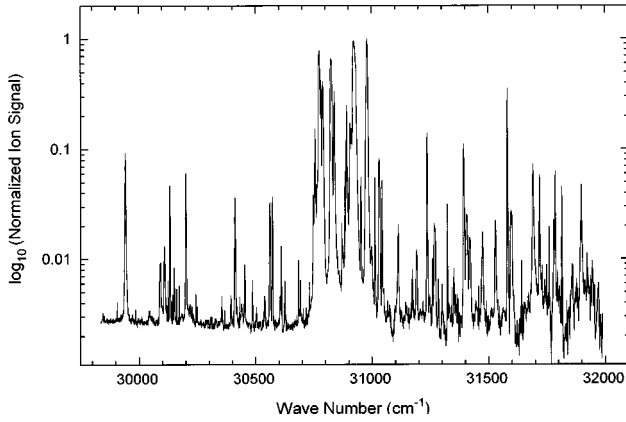


FIG. 2. One-color two-step resonance ionization spectrum of Ni I.

about 1000 at 58 amu. The mass selectivity allows an unambiguous assignment of all observed transitions to Ni I. A more elaborate description of the spectrometer will be given elsewhere [7].

Two pulsed laser systems (repetition rate of 10 Hz, pulse length of about 6 ns) are used. The first consists of a pulsed dye laser [Spectra-Physics (SP) PDL-3] in combination with

a wavelength extender (SP WEX-1), pumped by a neodymium-doped yttrium aluminum garnet (Nd:YAG) laser (SP GCR-12). With the laser dye DCM used and the KD*P frequency-doubling crystal, light with wavelengths between 313 and 335 nm and linewidths less than 0.4 cm^{-1} is generated. The second laser system consists of an optical parametric oscillator (SP MOPO-730) pumped by a Nd:YAG laser (SP GCR-230-10), yielding laser light tunable from 450 to 1600 nm with a 0.2-cm^{-1} linewidth. This laser light is also frequency doubled by KD*P crystals in a wavelength extender (SP WEX-1). The time overlap between the two laser pulses is controlled by a high precision digital delay generator (Stanford Research Systems DG535).

III. MEASUREMENTS AND DISCUSSION

A. One-color two-step resonant ionization of Ni I

In a first experiment the *one-color* two-step resonant ionization spectrum for Ni I in the wavelength interval between 313 and 335 nm was recorded. Laser light from the dye-laser system with an intensity of $\sim 15 \text{ MW/cm}^2$ was used. The ionization spectrum is shown in Fig. 2 and in Table I a list is given of those resonances observed with an ion signal larger

TABLE I. Resonances observed in the one-color two-step resonance ionization process of Ni I. In the first column the photon energy is given with an experimental error of 0.7 cm^{-1} . Resonance lines corresponding to known transitions [8,9] are identified in column two. An asterisk is printed for the transitions assigned as direct two photon transitions to autoionizing states (see Table III). Resonances marked with a double asterisk could not be identified. Relative intensities are given in the third column (within brackets for overlapping lines, see Fig. 2).

Photon energy (cm^{-1})	Resonance transition	Relative intensity	Photon energy (cm^{-1})	Resonance transition	Relative intensity
29 942.6	$b \ ^1D_2 \rightarrow \ ^3P_1^0$	0.09	30 979.7	$a \ ^3F_4 \rightarrow z \ ^3G_4^0$	(1.00)
30 132.6	**	0.05	31 012.9	*	0.05
30 201.1	$a \ ^1D_2 \rightarrow \ ^3F_2^0$	0.06	31 031.0	$a \ ^3F_4 \rightarrow z \ ^1F_3^0$	0.08
30 412.1	$b \ ^1D_2 \rightarrow \ ^3P_2^0$	0.04	31 043.5	*	0.05
30 561.8	$a \ ^3D_2 \rightarrow z \ ^1D_2^0$	0.03	31 111.3	**	0.02
30 572.4	$b \ ^1D_2 \rightarrow \ ^5D_2^0$	0.04	31 236.8	$a \ ^3D_3 \rightarrow z \ ^1D_2^0$	0.14
30 748.5	*	0.04	31 269.2	$a \ ^3D_1 \rightarrow z \ ^1P_1^0$	0.02
30 756.2	*	0.15	31 323.7	*	0.03
30 765.7	$a \ ^3F_2 \rightarrow z \ ^1P_1^0$	(0.05)	31 394.3	$a \ ^3F_2 \rightarrow \ ^3F_2^0$	0.11
30 773.3	**	(0.72)	31 407.5	$a \ ^3P_0 \rightarrow \ ^3D_1^0$	0.03
30 775.0	$a \ ^3D_3 \rightarrow z \ ^3G_4^0$	(0.78)	31 420.3	$a \ ^3P_2 \rightarrow \ ^3D_3^0$	0.02
30 781.8	*	(0.42)	31 474.1	$a \ ^3P_1 \rightarrow \ ^3P_1^0$	0.02
30 790.0	*	0.40	31 529.5	$a \ ^3P_2 \rightarrow \ ^3D_2^0$	0.02
30 823.7	*	(0.66)	31 581.4	$a \ ^3D_3 \rightarrow z \ ^3G_3^0$	0.36
30 826.2	$a \ ^3D_3 \rightarrow z \ ^1F_3^0$	(0.64)	31 594.8	$a \ ^3P_1 \rightarrow \ ^5S_2^0$	(0.03)
30 839.1	*	0.33	31 596.5	**	(0.03)
30 870.8	*	0.02	31 601.0	**	(0.03)
30 884.6	**	0.06	31 641.2	$a \ ^3F_3 \rightarrow \ ^3F_4^0$	0.01
30 891.4	*	0.25	31 690.8	$a \ ^3P_1 \rightarrow \ ^3D_1^0$	0.08
30 906.3	$a \ ^3D_2 \rightarrow z \ ^3G_3^0$	0.17	31 718.4	**	0.06
30 913.0	$a \ ^3P_2 \rightarrow \ ^3P_2^0$	(0.15)	31 760.1	**	0.02
30 921.5	*	(0.96)	31 780.2	$a \ ^3F_3 \rightarrow \ ^3F_3^0$	0.03
30 922.7	$a \ ^3F_4 \rightarrow z \ ^3G_5^0$	(0.96)	31 786.2	$a \ ^3F_4 \rightarrow z \ ^3G_3^0$	0.07
30 931.0	*	(0.59)	31 814.8	**	0.05
30 953.4	*	0.06	31 897.8	$a \ ^3D_1 \rightarrow \ ^3D_2^0$	0.05
30 974.2	*	(0.26)			

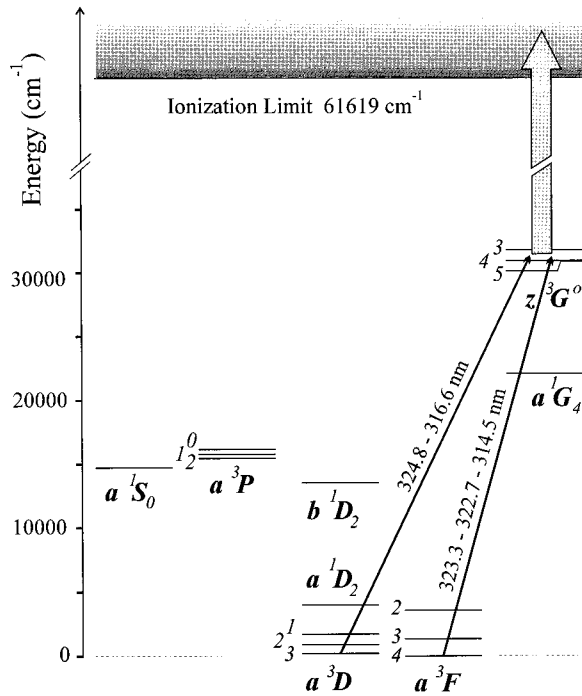


FIG. 3. Partial energy level scheme of Ni I, showing all metastable states and the triplet $z^3G_{3,4,5}^0$ used as intermediate levels in the two-color two-step ionization scheme. The transitions used as excitation steps are indicated.

than 1% of the strongest line. For the interpretation of these resonances, the metastable states of Ni I are presented in the lower part of Fig. 3.

All transitions tabulated in the literature [8,9] in the covered wavelength region that originate from the ground and low-lying metastable states are represented in the spectrum, together with some transitions originating from high-lying metastable states. They are identified in the second column of Table I. The population of high-lying states of Ni by sputtering will be discussed in Ref. [7]. Apart from the resonances corresponding to known atomic transitions, many relatively strong narrow lines show up that have not been observed before. These resonances will be discussed using the data of Sec. III B.

B. Structure of the Ni I continuum near the first ionization limit

A second series of experiments using *two-color* two-step RIS was performed to determine low-lying Ni I continuum states and their angular momentum. The experiments proceed in the following way. One laser is used to populate one of the $z^3G_J^0$ states lying just above half the ionization limit by tuning the wavelength to one of the atomic transitions $a^3F_4 \rightarrow z^3G_J^0$, or $a^3D_3 \rightarrow z^3G_J^0$ (see Fig. 3). A moderate laser pulse energy is used to limit the ion count rate by one-color two-step ionization. The second tunable laser is then employed with high energy fluence (~ 150 mJ/cm²) to ionize efficiently the excited atoms. The photon energy of this second step is scanned over an interval of about 3000 cm⁻¹ starting from the minimum energy required to ionize the excited atoms. As the second high-energy laser can resonantly ionize the ensemble of atoms in the ground and low-lying

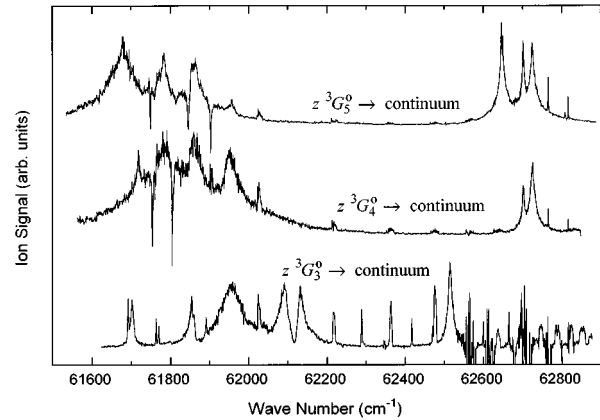


FIG. 4. The ionization spectra showing autoionizing states with $2 \leq J \leq 6$.

metastable states, a reference measurement is performed, under identical conditions, with light input only from the second laser. The difference between the two-color two-step and one-color two-step spectra then yields the continuum spectrum. Nevertheless, in the vicinity of the one-color resonances, the continuum spectrum remains very noisy.

In Fig. 4 experimental results are given for which the transitions $a^3F_4 \rightarrow z^3G_5^0$, $a^3D_3 \rightarrow z^3G_4^0$, and $a^3F_4 \rightarrow z^3G_3^0$ were used as excitation steps. From a direct comparison of the recorded spectra, the angular momenta of the autoionizing states can be determined. The use of $z^3G_{3,4,5}^0$ as intermediate states enables the determination of continuum states with angular momentum between $J=2$ and $J=6$.

In Table II the autoionizing states determined in this work, including their angular momentum as extracted from our measurements, are listed. Due to low statistics and overlapping lines in the spectra, some of the angular-momentum assignments are not completely unambiguous. For these states the most probable values are given in Table II within brackets. Also included in Table II is an indicative estimate of the width of the autoionizing states. The measured linewidths (w) are divided into three ranges: narrow ($w < 5$ cm⁻¹), intermediate (5 cm⁻¹ $< w < 20$ cm⁻¹), and wide ($w > 20$ cm⁻¹). The width of the experimental lines is, to a large extent, determined by the intensity of the ionizing laser pulse and therefore contains only indicative information on the lifetime of the continuum states. Different line shapes and widths for different spectra were observed for some autoionizing states and were found to be related to static Stark splitting in the extraction region. To our knowledge, none of the presently measured autoionizing states were identified or reported before.

The structure of the Ni I continuum can be used to complete the interpretation of the one-color two-step ionization spectrum. Some of the unidentified lines in the one-color spectrum show up at precisely half the energy of autoionizing states, or in other cases at precisely half the energy difference between an autoionizing state and a low-lying metastable state. These lines (indicated by an asterisk in Table I) can be explained as direct two-photon transitions to autoionizing states. The identified transitions are summarized in Table III in which the corresponding initial levels and autoionizing levels are given. Some of the unidentified lines in

TABLE II. Autoionizing states (energy E_{AI}) above the first ionization potential of Ni I. Angular momentum (J_{AI}) assignments are given in the second column. Uncertain assignments of the angular momenta are given within brackets (see text). Linewidths w are divided into three ranges: (I) if $w < 5 \text{ cm}^{-1}$, (II) if $5 \text{ cm}^{-1} < w < 20 \text{ cm}^{-1}$, and (III) if $w > 20 \text{ cm}^{-1}$. The experimental uncertainty of the energy of the listed states depends on the linewidth and is estimated to be 1 cm^{-1} for (I), 3 cm^{-1} for (II), and 6 cm^{-1} for (III).

$E_{AI} (\text{cm}^{-1})$	J_{AI}	w	$E_{AI} (\text{cm}^{-1})$	J_{AI}	w
61 680	6	III	62 091	2	III
61 692	2	I	62 131	2	II
61 702	3	II	62 217	4	II
61 719	(5)	II	62 288	2	I
61 763	(2)	I	62 363	4	II
61 766	(5)	III	62 417	2	I
61 770	(2)	I	62 475	4	II
61 784	5	III	62 514	2	II
61 793	(6)	III	62 567	4	II
61 855	(4)	III	62 647	6	II
61 859	(4)	III	62 702	(5)	II
61 869	(5)	III	62 725	5	II
61 891	(2)	I	62 765	5	I
61 904	(5)	II	62 808	6	I
61 955	4	III	62 816	5	I
62 025	4	II			

the studied frequency range could not be explained in this way (double asterisk in Table I). We did, however, only determine the autoionizing states in a relatively narrow energy range, and did not investigate autoionizing states with angular momenta $J \leq 1$ and $J \geq 7$. Therefore, for the unidentified lines an assignment as a direct two-photon transition to a continuum state cannot be excluded.

In order to obtain an estimate of the cross sections for direct two-photon ionization into autoionizing states, the ion yields as a function of laser intensity were measured. As an

example, the data for the transition at $30\,891.4 \text{ cm}^{-1}$ are given in Fig. 5. Using the photon flux dependence of the ion yields as a function of the generalized two-photon cross section σ_2 given in Ref. [10], this cross section turns out to be of the order of $\sigma_2 \approx 10^{-44} \text{ cm}^4 \text{ s}^{-1}$ (see Fig. 5). Generalized two-photon cross sections are expected to be of the order $\sigma_2 \approx 10^{-49} \text{ cm}^4 \text{ s}^{-1}$ [10]. The large enhancement we observed is due to the resonant excitation to an autoionizing state. The cross sections are further enlarged by the presence of intermediate states at nearly half the energy difference between

TABLE III. Direct two-photon transitions from low-lying states (angular momentum J_i) into autoionizing states (angular momentum J_{AI}). The last column gives the difference ΔE between the energy of the autoionizing state (E_{AI}) and twice the photon energy of the observed transition plus the energy of the initial state (E_i).

Photon energy (cm^{-1})	$E_i (\text{cm}^{-1})$	$E_{AI} (\text{cm}^{-1})$	J_i	J_{AI}	$\Delta E (\text{cm}^{-1})$
30 748.5	205	61 702	3	3	0.0
30 756.2	205	61 719	3	(5)	-1.6
30 781.8	205	61 766	3	(5)	2.6
30 790.0	205	61 784	3	5	1.0
30 823.7	205	61 855	3	(4)	-2.6
30 839.1	0	61 680	4	6	-1.8
30 870.8	205	61 955	3	4	-8.4
30 891.4	0	61 784	4	5	-1.2
30 921.5	0	61 855	4	(4)	-12
30 931.0	0	61 859	4	(4)	3.0
30 953.4	0	61 904	4	(5)	2.8
30 974.2	0	61 955	4	4	-6.6
31 012.9	0	62 025	4	4	-0.2
31 043.5	0	62 091	4	2	-4.0
31 259.0	205	62 725	3	5	-1.2
31 323.7	0	62 647	4	6	0.4

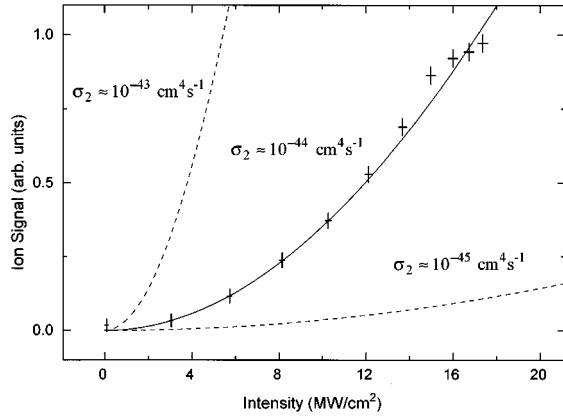


FIG. 5. Intensity dependence of the ion signal for the two-photon transition at $30\,891.7\text{ cm}^{-1}$ and generalized cross section fittings.

the ground state and the autoionizing state, which also enhances the strength of the two-photon transition. For three-level systems in a single-frequency field, this type of excitation has been treated theoretically by, e.g., Cantrell *et al.* [11] and Letokhov [3]. However, in our case, with the third level situated above the ionization limit and with the presence of several close by intermediate states, a quantitative description becomes very cumbersome, and is beyond the scope of the present paper.

C. Ionization cross sections

The presence of autoionizing states will strongly influence the ionization cross sections for certain *two-step* RIS processes. We measured ionization saturation curves and deduced cross sections for one-color two-step processes and for two-color two-step processes with the ionization step tuned to an autoionizing state. For the latter measurement the excitation step was saturated completely, which is obtained already at moderate laser flux. The saturation curves are given in Figs. 6 and 7.

Since the linewidth of the lasers is large, coherent processes are absent, and the ionization rate from the intermediate level into the continuum can be described within the rate equation approach. Assuming that the transition between the bound states is saturated, the ionization rate approaches saturation exponentially with the laser fluence (the number of photons per unit area) [2,3]. If the spatial distribution of the laser fluence $\phi(r)$ is taken into account, the total number of created photoions per pulse N_i is given by

$$N_i = \int dV n_0 \{1 - \exp[-\frac{1}{2} \sigma_i \phi(r)]\}, \quad (1)$$

with n_0 the initial density of atoms on the quantum states probed by the ionizing laser and σ_i the photoionization cross section.

The spatial intensity distribution of the ionizing laser was measured by intersecting the beam with a movable knife edge in two perpendicular directions [12]. The beam has an elliptical shape and a near-Gaussian intensity profile along the major and minor axes. We first considered the commonly used approximation that consists in assuming a constant laser

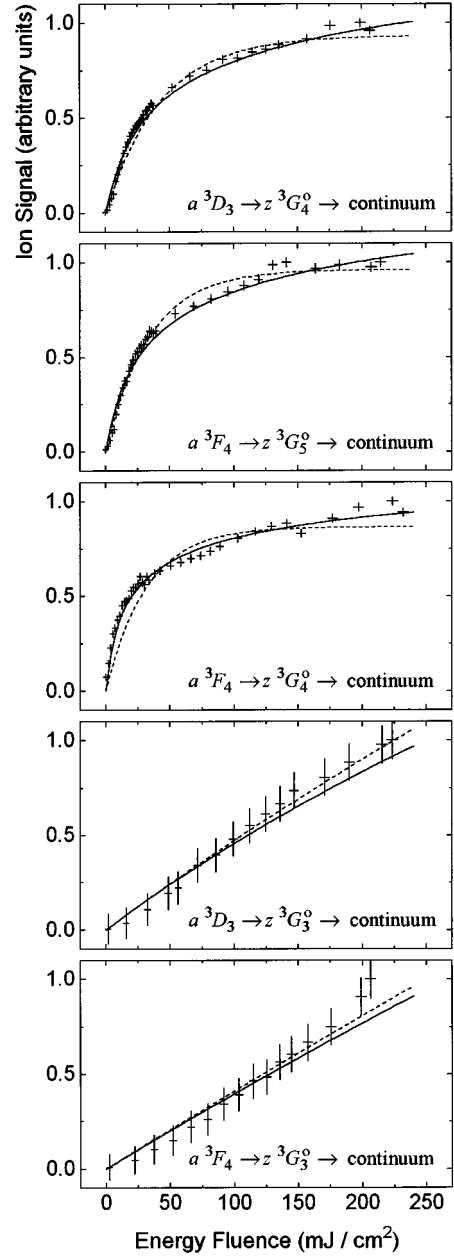


FIG. 6. Saturation behavior of one-color two-step resonance ionization. Cross section fittings using Eq. (2) (dashed line) and Eq. (3) (full line) are included.

fluence over an elliptical area determined by the measured $1/e$ points (R_x and R_y) and zero outside this area [13]. This results in

$$N_i = N_0 [1 - \exp(-\frac{1}{2} \sigma_i \Phi)], \quad (2)$$

with Φ the fluence calculated from the total number of photons in the pulse $\pi R_x R_y \Phi$ determined by the measured total energy in the pulse. Approximation (2) is, however, too crude, since it results in poor fits to the saturation data, as can be seen from Fig. 6.

Therefore we divided the beam into five areas: an inner elliptical area with semiaxes $\frac{1}{4}R_x$ and $\frac{1}{4}R_y$ surrounded by four elliptical rings with outer border semiaxes $\frac{1}{2}(i + \frac{1}{2})R_x$,

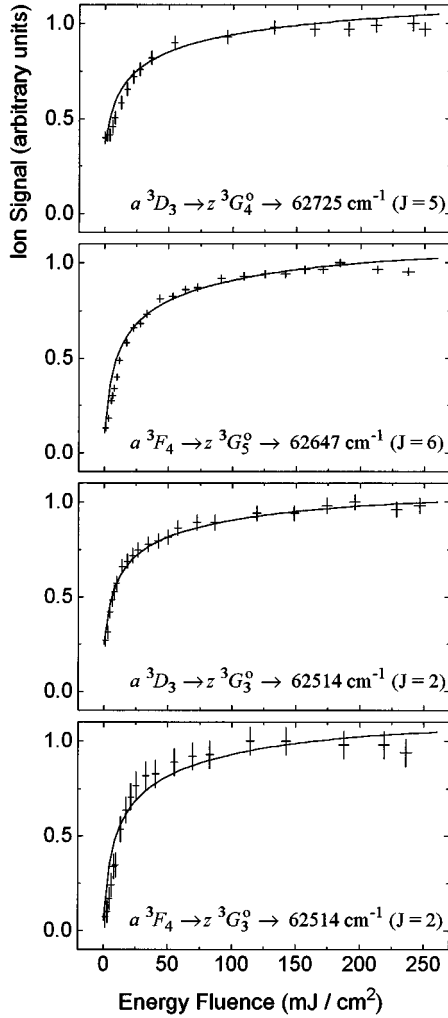


FIG. 7. Saturation behavior of two-color two-step resonance ionization. The ionization step is tuned in resonance from the intermediate state to an autoionizing state. Cross section fittings using Eq. (3) are included.

$\frac{1}{2}(i + \frac{1}{2})R_y$, where $i=1,2,3,4$ [14]. The fluences in these areas, according to the Gaussian distribution, are then Φ , 0.78Φ , 0.37Φ , 0.11Φ , and 0.02Φ and expression (2) can be replaced by

$$N_i = \frac{16}{81} N_0 \left\{ \frac{1}{16} \left[1 - \exp\left(-\frac{1}{2} \sigma_i \Phi\right) \right] + \frac{1}{2} \left[1 - \exp\left(-\frac{0.78}{2} \sigma_i \Phi\right) \right] + \left[1 - \exp\left(-\frac{0.37}{2} \sigma_i \Phi\right) \right] + 1.5 \left[1 - \exp\left(-\frac{0.11}{2} \sigma_i \Phi\right) \right] + 2 \left[1 - \exp\left(-\frac{0.02}{2} \sigma_i \Phi\right) \right] \right\}. \quad (3)$$

This expression provides good fits to the saturation curves, as can be seen from Figs. 6 and 7, and has therefore been used to extract the ionization cross sections. (It should be mentioned that accounting for the spatial distribution of the fluence is very important, as not doing so would, in our case, result in cross sections 5 to 10 times too small.)

The derived ionization cross sections with errors stemming from the fitting procedure are presented in Table IV. An additional systematic error in the cross section values is induced by deviations from a Gaussian profile of the laser spot and is estimated to be about 20%. The error due to the approximation of Eq. (3) is negligible with respect to the fitting error and the systematic error. This was verified by modifying Eq. (3) for different numbers of areas, resulting in only minor changes in the fitted cross sections.

For nonresonant ionization from the intermediate states into a structureless continuum, these cross sections are expected to be of the order of 10^{-18} cm^2 [2,3]. The values we determined are clearly depending on the resonant character of the ionization step. For one-color ionization, the very high ionization cross section at the frequency of the transition $a \ ^3F_4 \rightarrow z \ ^3G_4^0$, arriving in the continuum at $61\ 959 \text{ cm}^{-1}$, is due to an almost exact double resonant process to the autoionizing state at $61\ 955 \text{ cm}^{-1}$ ($J=4$). Similarly the cross sections at the frequencies of the transitions $a \ ^3D_3 \rightarrow z \ ^3G_4^0$ and $a \ ^3F_4 \rightarrow z \ ^3G_5^0$ are enhanced by the presence of autoionizing states at $61\ 766 \text{ cm}^{-1}$ ($J=5$) and at $61\ 855 \text{ cm}^{-1}$ ($J=4$), respectively (see Tables I and II). The much lower ionization cross section, if the transitions $a \ ^3F_4 \rightarrow z \ ^3G_3^0$ and $a \ ^3D_3 \rightarrow z \ ^3G_3^0$ are used as excitation steps, can be explained by the absence of an autoionizing state at twice the energy of the excitation transition (plus the energy of the $a \ ^3D_3$ state in the latter case).

TABLE IV. Cross sections determined from the saturation curves of Figs. 6 and 7. Fitting results using a Gaussian laser beam profile [Eq. (3)] are given for one-color and two-color two-step ionization. Apart from the quoted fitting errors, an additional systematic error of 20% has to be taken into account (see text). For the two-color values, the ionizing laser frequency is tuned to an autoionizing state.

Excitation transition	One-color two-step		Two-color two-step	
	Ionization transition	σ_i (cm ²)	Ionization transition	σ_i (cm ²)
$a \ ^3D_3 \rightarrow z \ ^3G_4^0$	$z \ ^3G_4^0 \rightarrow 61755 \text{ cm}^{-1}$	$1.6(2) \times 10^{-16}$	$z \ ^3G_4^0 \rightarrow 62725 \text{ cm}^{-1}$ ($J=5$)	$4.1(7) \times 10^{-16}$
$a \ ^3F_4 \rightarrow z \ ^3G_5^0$	$z \ ^3G_5^0 \rightarrow 61845 \text{ cm}^{-1}$	$2.0(2) \times 10^{-16}$	$z \ ^3G_5^0 \rightarrow 62647 \text{ cm}^{-1}$ ($J=6$)	$6.3(4) \times 10^{-16}$
$a \ ^3F_4 \rightarrow z \ ^3G_4^0$	$z \ ^3G_4^0 \rightarrow 61959 \text{ cm}^{-1}$	$4.0(4) \times 10^{-16}$		
$a \ ^3D_3 \rightarrow z \ ^3G_3^0$	$z \ ^3G_3^0 \rightarrow 63368 \text{ cm}^{-1}$	$5.5(6) \times 10^{-18}$	$z \ ^3G_3^0 \rightarrow 62514 \text{ cm}^{-1}$ ($J=2$)	$5.9(7) \times 10^{-16}$
$a \ ^3F_4 \rightarrow z \ ^3G_3^0$	$z \ ^3G_3^0 \rightarrow 63572 \text{ cm}^{-1}$	$1.7(3) \times 10^{-18}$	$z \ ^3G_3^0 \rightarrow 62514 \text{ cm}^{-1}$ ($J=2$)	$6.5(8) \times 10^{-16}$

The enhancement of the ionization efficiency for two-color two-step processes by making use of autoionizing states, is clearly demonstrated by the measured cross sections. For the processes with transitions $a^3D_3 \rightarrow z^3G_3^0$ and $a^3F_4 \rightarrow z^3G_3^0$ as excitation steps, the ionization cross section is about a factor 100 larger if the frequency of the second step is tuned resonantly to an autoionizing state. This enhancement is evidently much less pronounced for the processes using the transitions $a^3D_3 \rightarrow z^3G_4^0$ and $a^3F_4 \rightarrow z^3G_5^0$, since there the frequency of the excitation step is also nearly resonant for the ionization step. For the transition $a^3F_4 \rightarrow z^3G_4^0$ the exact double resonant nature of the one-color scheme made a saturation measurement for two-color ionization even impossible.

IV. CONCLUSIONS

Two-step resonant photoionization of sputtered Ni atoms has been studied using one-color and two-color processes with photon energies around half the ground-state ionization energy. Two-color resonance ionization from the ground state a^3F_4 and the first excited state a^3D_3 via the triplet $z^3G_{3,4,5}^0$, revealed the existence of a large number of autoionizing states with angular momentum between 2 and 6 in

the energy region from 61 680 to 62 800 cm^{-1} .

The measured one-color resonance ionization spectrum of Ni I between 313 and 335 nm contains a number of untabulated lines. With the knowledge of the continuum structure, we can identify most of them as direct two-photon transitions starting from low-lying metastable states and reaching autoionizing states.

We measured the saturation behavior for selected two-step ionization channels from which the cross sections for photoionization are deduced, yielding two orders of magnitude higher cross sections if autoionizing states are involved. Due to the near resonant ionization into autoionizing states, the cross sections for several one-color ionization channels are only slightly smaller than the cross sections obtained for two-color processes.

ACKNOWLEDGMENTS

This work is financially supported by the Belgian National Fund for Scientific Research (NFWO) and the Flemish Concerted Action (GOA) and Inter-University Attraction Pole (IUAP) Programs. P. L. would like to thank the NFWO for financial support.

-
- [1] M. G. Payne, Lu Deng, and N. Thonnard, *Rev. Sci. Instrum.* **65**, 2433 (1994).
- [2] G. S. Hurst and M. G. Payne, *Principles and Applications of Resonance Ionization Spectroscopy* (Institute of Physics, Bristol, 1988).
- [3] V. S. Letokhov, *Laser Photoionization Spectroscopy* (Academic, Orlando, FL, 1987).
- [4] Z. N. Qamhieh, E. Vandeweert, R. E. Silverans, P. Van Duppen, M. Huyse, and L. Vermeeren, *Nucl. Instrum. Methods B* **70**, 131 (1992).
- [5] L. Vermeeren, N. Bijmens, M. Huyse, Y. A. Kudryavtsev, P. Van Duppen, J. Wauters, Z. N. Qamhieh, P. Thoen, E. Vandeweert, and R. E. Silverans, *Phys. Rev. Lett.* **73**, 1935 (1994).
- [6] E. Vandeweert, P. Thoen, Z. N. Qamhieh, P. Lievens, and R. E. Silverans, in *Proceedings of the Seventh International Symposium on Resonance Ionization Spectroscopy, Bernkastel-Kues, Germany, 1994*, edited by H.-J. Kluge, J. E. Parks, and K. Wendt, AIP Conf. Proc. No. 329 (AIP, Woodbury, NY, 1995), p. 91.
- [7] E. Vandeweert *et al.* (unpublished).
- [8] *Spectroscopic Data for Titanium, Chromium, and Nickel, Volume 3: Nickel*, edited by W. L. Wiese and A. Musgrove (Controlled Fusion Atomic Data Center, Oak Ridge National Laboratory, Oak Ridge, TN, 1989).
- [9] U. Litzén, J. W. Brault, and A. P. Thorne, *Phys. Scr.* **47**, 628 (1993).
- [10] J. Morellec, D. Normand, and G. Petite, *Adv. At. Mol. Phys.* **18**, 98 (1982).
- [11] C. D. Cantrell, V. S. Letokhov, and A. A. Makarov, in *Coherent Nonlinear Optics*, edited by M. S. Feld and V. S. Letokhov (Springer-Verlag, Berlin, 1980), p. 165.
- [12] R. V. Ambartsumian, V. M. Apatin, V. S. Letokhov, A. A. Makarov, V. I. Mishin, A. A. Pureskii, and N. P. Furzikov, *Zh. Eksp. Teor. Fiz.* **70**, 1660 (1976) [*Sov. Phys. JETP* **43**, 866 (1976)].
- [13] C. E. Burkhardt, J. L. Libbert, Jian Xu, J. J. Leventhal, and J. D. Kelly, *Phys. Rev. A* **38**, 5949 (1988).
- [14] L. Vermeeren, Annex-thesis, Katholieke Universiteit Leuven (unpublished).